Applied Catalysis B: Environmental 182 (2016) 550–561

Contents lists available at ScienceDirect

Applied Catalysis B: Environmental

journal homepage: www.elsevier.com/locate/apcatb

Studies on the influence of H_2S and SO_2 on the activity of a PdO/Al_2O_3 catalyst for removal of oxygen by total oxidation of (bio-)methane at very low O_2:CH_4 ratios

Felix Ortloff[a,*], Jan Bohnau[a], Utz Kramar[b], Frank Graf[a], Thomas Kolb[a,c]

[a] DVGW Research Center at Engler-Bunte-Institute (DVGW-EBI), Karlsruhe Institute of Technology (KIT), Engler-Bunte-Ring 1, 76131 Karlsruhe, Germany
[b] Institute of Mineralogy and Geochemistry (IMG), Karlsruhe Institute of Technology (KIT), Adenauerring 20, 76131 Karlsruhe, Germany
[c] Engler-Bunte-Institute, Fuel Technology Division (EBI ceb), Karlsruhe Institute of Technology (KIT), Engler-Bunte-Ring 1, 76131 Karlsruhe, Germany

ARTICLE INFO

Article history:
Received 29 June 2015
Received in revised form 4 September 2015
Accepted 12 September 2015
Available online 14 September 2015

Keywords:
Catalytic combustion
$PdO/Al2O_3$ catalyst
Sulfur contaminants
Deactivation
In-situ regeneration

ABSTRACT

This work focuses on the deactivation and in-situ regeneration effects of a commercial PdO/Al_2O_3 catalyst for removal of oxygen by oxidation of CH_4 at low O_2:CH_4 ratios when hydrogen sulfide and sulfur dioxide are applied to the gas stream. The experimental work is carried out at an operating temperature range of 200 °C < T < 300 °C, atmospheric pressure and H_2S/SO_2 contents of <100 ppmv.

SO_2 and H_2S show a different behavior in the examined range of operating conditions. Due to the low operating temperatures and low oxygen contents applied in this work, it was possible to identify an intermediate species, presumably $PdSO_3$, with an increased activity for the oxidation of methane. This stands in contrast to the literature, where SO_2 is typically seen to cause catalyst deactivation. Based on the experimental results, a reaction scheme was derived and kinetic measurements for each of the participating reactions were carried out separately.

Furthermore, a deactivation model was derived and validated by experimental data with low contents of H_2S, showing that residual activities, as observed by some authors, are a result of rate-equality of deactivation and in-situ regeneration process on the surface of the catalyst.

1. Introduction

In order to prevent damage to the natural gas infrastructure (e.g., by corrosion [1]), the maximum oxygen concentration is limited to 10 ppmv for transportation pipelines connected to underground storages and/or cross border transmission [2–4]. One option for the removal of oxygen from biomethane, which is to be fed into the natural gas grid, (or other fuel gas streams) is the implementation of the heterogeneously catalyzed oxidation reaction of methane (Eq. (1)), catalyzed by PdO/Al_2O_3.

$$CH_{4,(g)} + 2O_{2,(g)} \rightarrow CO_{2,(g)} + 2H_2O_{(l)} \quad \Delta_R H^\theta = -890.5\,\text{kJ/mol} \quad (1)$$

Typically, the catalytic oxidation reaction of methane is applied in lean-gas treatment, in terms of reduction of CH_4 emissions from (oxygen-rich) off-gas streams [5] and in catalytic burning systems for increased combustion efficiencies [6–8]. In contrast to these applications, catalytic removal of oxygen from fuel gas streams is carried out at oxygen-understochiometric conditions and consequently at lower reaction temperatures [8–10].

In Biomethane no hydrogen or hydrocarbons are present. Therefore, the utilization of CH_4 brings in economic benefits in comparison with state-of-the-art technologies for oxygen removal, as no additional reducing agent has to be supplied, stored and added to the gas separately. Besides, the utilization of biomethane for removal of oxygen is a more sustainable option than using fuels from fossil sources [11,12].

Recently, kinetic data for the catalytic removal of oxygen by combustion of CH_4 for very low O_2:CH_4 ratios was determined

Abbreviations: ads, adsorbed; BTEX, benzene, toluene, ethylbenzene, and xylenes; calc, calculated; exp, experimental; (g), gaseous state; GHSV, gas hourly space velocity; (l), liquid state; ppmv, parts per million (volumetric); STP, standard temperature pressure; TBM, tert-butyl-mercaptane; THT, tetrahdyrothiophene; TOS, time on stream; TPD, temperature programmed desorption; XRF, X-ray fluorescence (analysis); LiF200, diffraction crystal used for wavelength separation in X-ray fluorescence for short wavelength (LiF crystal cut along the lattice plane 200, lattice distance 2d = 4.028 Å = 0.4028 nm); PET, pentaerythrit crystal (lattice distance 2d = 8.74 Å, intermediate wavelength); XS55, synthetic W-Si multilayer crystal (lattice distance 2d = 55 Å, long wavelength).

* Corresponding author.
E-mail address: ortloff@dvgw-ebi.de (F. Ortloff).

http://dx.doi.org/10.1016/j.apcatb.2015.09.026
0926-3373/

Nomenclature

Θ	surface coverage (–)
A-D	kinetic constants (–)
a	activity (–)
d	deactivation order (–)
E_A	activation energy (kJ/mol)
$\Delta_R H^\Theta$	standard enthalpy of reaction (kJ/mol)
$\Delta_{ads} H^\Theta$	standard enthalpy of adsorption (kJ/mol)
k	reaction rate constant (as applied)
K	equilibrium constant (bar^{-C}; bar^{-D})
$K\beta'/K\beta_{1,3}$	XRF intensity ratio (–)
I/I_{max}	xray intensity ratio (–)
2ϑ	Bragg-diffraction angle (°)
m_{ac}	mass of active compound (g)
m, n	reaction orders (–)
N_i	amount of species i (mol)
p_i	(partial) pressure (of i) (bar)
Ψ	deactivation function (as applied)
ϕ_i	ratio i of total active sites (–)
r_i	mass specific reaction rate (mol/(s g))
R	universal gas constant 8.314 (kJ/(kmol K))
t	time (s)
T_R	reaction temperature (°C)
$\dot{V}$	volumetric flow rate (m^3/s)
X_i	conversion of i (–)
y_i	mole fraction of i in the gas phase (–)

for a set of reference catalysts on noble metal basis (platinum and palladium on Al_2O_3 support) [41].

Furthermore, the effects of trace compounds of biomethane on catalyst durability are of interest, e.g., sulfur components, siloxanes [13], ammonia [8], BTEX [14] and halogenated hydrocarbons [15]. This work focuses on sulfur compounds, as they represent the major part of contaminants of biomethane [16].

In the majority of available literature, the influence of H_2S and SO_2 [17–19] on the activity of noble metal catalysts for catalytic combustion of methane is studied. Deactivation by SO_2 or H_2S are usually not treated separately [20], since under typical reaction conditions of methane combustion (T > 350 °C, oxygen excess) hydrogen sulfide is oxidized to SO_2 [21]. When mercaptanes [10] or THT (Tetrahdyrothiophene) [22] are examined, typically a complete conversion to H_2O, CO_2 and SO_2 is assumed, since C—S bonds are not stable at high temperatures [23,24]. The deactivation mechanism is thus treated as of SO_2.

Despite extensive research on the deactivation and regeneration mechanism of sulfur compounds on noble catalysts [18,19,25,26], the details of the catalytic surface processes do not seem to be fully understood yet (see Section 2). Due to the lack of data on the influence of sulfur contaminants on catalyst activity at low O_2:CH_4 ratios, detailed examinations on sulfur poisoning of a PdO/Al_2O_3 catalyst under oxygen removal conditions have been carried out in this work.

2. Literature overview

In literature, there is general agreement, that sulfur compounds cause significant loss of catalyst activity, when noble metals on Al_2O_3 are applied. Deactivation of the catalyst is initiated by adsorption of the sulfur-containing compound on the catalyst surface, followed by a chemical reaction with the active compound. Due to the chemisorption reaction, sulfur forms chemical bonds with the active sites hindering desorption at typical operating conditions. Gradually, the catalyst is poisoned [17,25].

In some cases [17,20,25,26], residual activities of fully poisoned PdO/Al_2O_3 catalysts are observed. Two explanations can be found for this effect:

- The sulfur covered active compound ($PdSO_x$) itself features some catalytic activity for methane oxidation [17,26] or
- a continuous regeneration of the active sites takes place, caused by storage of sulfur in the catalyst support under formation of $Al_2(SO_4)_3$ [25].

Ordonez et al. [26] examined the influence of SO_2 on the catalytic activity of PdO/Al_2O_3. As feed gas, 5000 ppmv of methane in an air stream was used. The reaction was operated in a temperature range of 350–550 °C. Ordonez et al. found that high sulfur concentrations lead to an increase in deactivation rate, whereas the residual activity of the catalyst remains constant. Further, an increase of reaction temperature had a positive effect on the residual activities in Ordonez's case. Unfortunately, Ordonez et al. did not commit to one of the two aforementioned explanations for their observations. For modelling, the authors assumed $PdSO_4$ to cause the residual activities.

Besides the active compound, the catalyst support plays an important role for the deactivation of noble metal catalysts. Hoyos et al. [17] showed that the deactivation rate of PdO on an Al_2O_3 support is significantly lower than on SiO_2, which is a consequence of the sulfate forming ability of the support material. Al_2O_3 is able to store sulfur as $Al_2(SO_4)_3$ and therefore acts as a sulfur sink, causing a decrease in deactivation rate. Hoyos et al. proved the existence of sulfate by infrared-spectroscopy. In contrary, SiO_2 was not able to form sulfate. Escandón et al. [27] confirmed these results.

Yu and Shaw [18] also examined the deactivation of a PdO/Al_2O_3 with H_2S in excess of oxygen. From their own results and from literature data the authors proposed a deactivation mechanism of three consecutive reaction steps—the formation of sulfide (Eq. (2)), its oxidation to sulfite (Eq. (3)) and finally the storage of sulfur as sulfate in the catalyst support (Eq. (4)):

$$PdO + H_2S \rightarrow PdS + H_2O \quad (2)$$

$$PdS + 1.5O_2 \rightarrow PdSO_3 \quad (3)$$

$$3PdSO_3 + Al_2O_3 + 1.5O_2 \rightarrow 3PdO + Al_2(SO_4)_3 \quad (4)$$

The authors found that at 200 °C the oxidation of sulfide to sulfite (Eq. (3)) is kinetically inhibited. As a consequence, PdS remains on the catalytic surface at low temperatures. At higher temperatures (400 °C) and in presence of oxygen, the oxidation of sulfide to sulfite occurs. Thereafter, aluminum sulfate is formed and the active compound of the catalyst (PdO) is restored (Eq. (4)). Yu and Shaw carried out infrared spectroscopy measurements and did not observe any formation of $PdSO_4$. Yu and Shaw further claimed physical blockage of the active sites by $Al_2(SO_4)_3$ and a decrease of surface area (BET) responsible for the short-term deactivation of the catalyst at high temperatures.

Other research groups [17,19,25] do not share this view and rather explain the short-term deactivation by transformation of PdO to any $PdSO_x$ species with less activity. Ordonez et al. [28] investigated the deactivation and regeneration of PdO/Al_2O_3-catalysts after SO_2-poisoning by performing desorption experiments under inert atmosphere at high temperatures (600 °C). Under these conditions, both, O_2 and SO_2 can be detected in the off-gas in various ratios. This indicates for the presence of SO_x-groups on the active sites of the catalyst, as $PdSO_4$ decomposes to SO_2 and O_2 (Eq. (10)) at high temperatures. After high temperature deactivation experiments, an increasing amount of oxygen is released due to a higher degree of sulfate formation (Eq. (6)). As a conclusion, Ordonez et al. assumed that both, sulfate and sulfite groups,

Table 1
Gases used with information on respective purities.

Compound	Purity
Methane	3.5 (99.95 vol%)
Synthetic air (20.5 vol% O_2 in N_2)	20.5 vol% O_2 in N_2 5.0
Nitrogen	5.0 (99.999 vol%)
Hydrogen	5.0 (99.999 vol%)
Hydrogen sulfide in methane	300 ppmv in CH_4 5.0
Sulfur dioxide in nitrogen	1370 ppmv in N_2 5.0

are present on the catalyst surface and proposed the mechanism Eqs. (5)–(12).

$$PdO + SO_2 \rightarrow PdSO_3 \quad (5)$$

$$PdO + SO_2 + 0.5O_2 \rightarrow PdSO_4 \quad (6)$$

$$3PdSO_3 + Al_2O_3 \rightarrow 3PdO + Al_2(SO_3)_3 \quad (7)$$

$$3PdSO_4 + Al_2O_3 \rightarrow 3PdO + Al_2(SO_4)_3 \quad (8)$$

$$PdSO_3 \rightarrow PdO + SO_2 \quad (9)$$

$$PdSO_4 \rightarrow PdO + SO_2 + 0,5O_2 \quad (10)$$

$$Al_2(SO_3)_3 \rightarrow Al_2O_3 + 3SO_2 \quad (11)$$

$$Al_2(SO_4)_3 \rightarrow Al_2O_3 + 3SO_2 + 1.5O_2 \quad (12)$$

Furthermore, Ordonez et al. examined different gases and gas mixtures for their ability to regenerate a poisoned Pd catalyst. A catalyst, which afore was deactivated with SO_2, was regenerated at 550 °C with hydrogen, dry air, humid air, nitrogen and under vacuum for 20 h. Exclusively with hydrogen a complete recovery of catalyst activity was achieved. For the other gases, only 80–90% of the original activity was reached.

3. Experimental set-up and procedure

An extensive description of the lab-scale test rig used in this work is given in [41]. The palladium catalyst used in this work is a commercially available product. As active compound 0.5 wt% of Pd are dispersed on the spherical catalyst support of Al_2O_3 with an outer diameter of 1–1.2 mm. The catalyst features a specific surface area of 173 m^2/g (BET). During the measurements, the catalyst was diluted with glass-spheres of similar diameter by a ratio of 1:10. The glass-spheres are chemically inert with respect to chemical adsorption of sulfur compounds. Information on the applied experimental procedures is given in relevant subsections. Table 1 gives an overview over the applied gases. For gas analysis an appropriate μGC system (Agilent F490; MSA5 and PPQ columns; TCD) was used. Additionally, representative catalyst samples were prepared under relevant test conditions and analyzed ex-situ via XRF (details on XRF methodology are given in Section 3.1). The kinetic parameters and reaction orders were determined by numeric fit via minimization of least squares of integral experimental and calculated oxygen conversion. The catalytic reactor was modelled as a PFR (Bo > 100). MS Excel was used for computation.

3.1. XRF-analysis

Principles of X-ray fluorescence analysis are described in [29,30]. The determination of sulfur species on the catalyst surface was carried out by Kβ-X-ray fluorescence with representative samples, taken subsequently to the measurements in the catalytic test rig. The intensity ratio of $K\beta'/K\beta_{1,3}$ varies depending on the binding form of S and can be used for speciation analysis [31–34]. At the Kα-line a small energy shift in dependence of the binding form can be observed when spectrometers with an extremely good angle resolution are used [35].

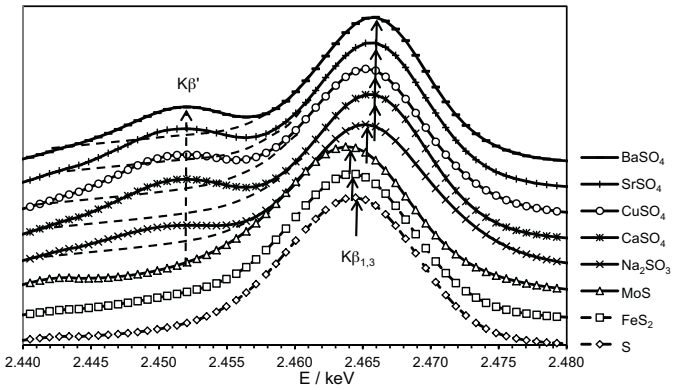

Fig. 1. Energy scan across the $K\beta_{1,3}$ and Kβ′- lines of elementary sulfur, sulfide, sulfite and different sulfates. The spectra are normalized to the maximum intensity point and shifted for clarity.

Table 2
$K\beta'/K\beta_{1,3}$ intensity ratio for sulfides, sulfites and sulfates. The intensity ratio of elementary sulfur at the Kβ′ position to the $K\beta_{1,3}$ intensity was set as zero point.

Compound	$K\beta'/K\beta_{1,3}$ intensity ratio
S	–
FeS_2	0.03
MoS	0.023
Na_2SO_3	0.143
$CaSO_4$	0.276
$CuSO_4$	0.268
$SrSO_4$	0.269
$BaSO_4$	0.242

The measurements were carried out, using an S4 Explorer (Bruker AXS, acc.: 0.05% F.S.) equipped with Rh-tube, and the crystals LiF200 (2d = 4.028 Å), PET (2d = 8.74 Å) and XS55 (2d = 55 Å). The PET was used for the determination of the sulfur speciation. The Kβ-region was scanned from 69.5° to 71° 2ϑ equivalent to 2.4851–2.4396 keV (step size ~0.73 eV) to determine the $K\beta'/K\beta_{1,3}$ intensity ratio. For noise reduction the scans were smoothed using a moving 13 point polynomial approximation [36]. The samples were prepared in spectro cups, covered with 6 μm mylar film as bulk powder samples. For calibration of the peak position and the $K\beta'/K\beta_{1,3}$ intensity ratios the following sulfur species were measured: elemental sulfur, FeS_2, MoS, Na_2SO_3, $CaSO_4$ x $2H_2O$, $CuSO_4$, $SrSO_4$, and $BaSO_4$. The Kβ scans of these compounds are shown in Fig.1.

With elementary sulfur and sulfides the Kβ′-line is not present. With increasing oxidation state of sulfur the $K\beta'/K\beta_{1,3}$ intensity ratio increases. The observed energy difference between the Kβ′ and the $K\beta_{1,3}$-line is ~15 eV. This is in agreement with the data of [31]. Table 2 compiles the $K\beta'/K\beta_{1,3}$ intensity ratio for the different compounds.

4. Results and discussion

In order to determine whether one of the aforementioned deactivation mechanisms is applicable to the reaction conditions applied in this work (low O_2:CH_4 ratios), preliminary measurements on each of the involved reaction steps have been carried out (Sections 4.1.1–4.2.1). Based on these findings, a reaction scheme is proposed (Section 4.3) and a deactivation/reactivation model is applied (Section 4.4).

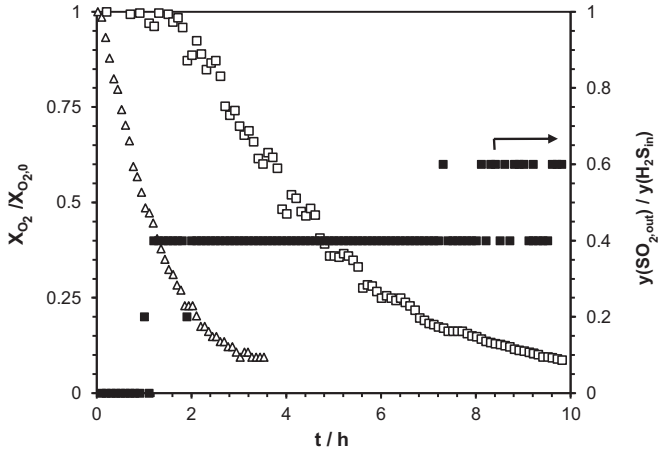

Fig. 2. Preliminary examinations on the deactivation of PdO/Al_2O_3 by hydrogen sulfide ($\dot{V}$ = 100 l/h (STP), $p_{CH_4,0}$ = 960 mbar, GHSV: 45,000 h^{-1}, p_{total} = 1.013 bar, $y_{O_2,0}$ = 4,100 ppmv, $y_{H_2S,0}$ = 50 ppmv, balance: N_2): T = 250 °C (Δ); T = 300 °C (□).

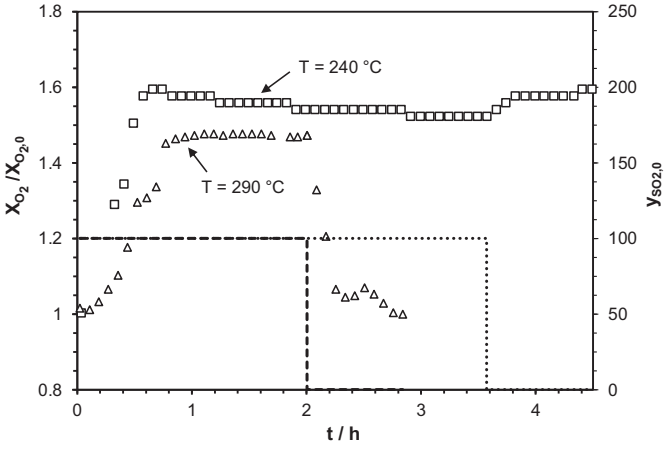

Fig. 3. Influence of sulfur dioxide on oxygen conversion at different temperatures ($\dot{V}$ = 100 l/h (STP), $p_{CH_4,0}$ = 960 mbar, GHSV: 45,000 h^{-1}, p_{total} = 1.013 bar, balance: N_2): T = 240 °C, $y_{O_2,0}$ = 1,025 ppmv, $X_{O_2,0}$(240 °C) = 0.6; (□); T = 290 °C, $y_{O_2,0}$ = 4,100 ppmv (Δ), $X_{O_2,0}$(290 °C) = 0.67; $y_{SO_2,0}$ at T = 240 °C (. . .); $y_{SO_2,0}$ at T = 290 °C: (---).

4.1. Examinations on reaction mechanism

4.1.1. Deactivation of PdO/Al_2O_3 by hydrogen sulfide and sulfur dioxide

Fig. 2 shows two deactivation experiments with H_2S in the feed at different temperatures (250 °C and 300 °C). For comparison, the actual oxygen conversion X_{O_2} is normalized to the conversion of the fresh catalyst $X_{O_2,0}$. While the catalyst shows activity for methane oxidation, no H_2S is detected at the reactor outlet.

During both experiments a decrease of oxygen conversion can be observed due to formation of palladium sulfide [18], as confirmed by XRF measurements (see Section 4.1.3).

Furthermore, it is obvious that the catalyst deactivates faster at 250 °C than at 300 °C. At 250 °C, after 3.5 h no carbon dioxide is detected in the off-gas anymore—methane conversion is stopped completely. The residual oxygen conversion ($X_{O_2,res}$) probably is a result of oxidation of hydrogen sulfide to water and surface sulphur species and some beginning of regeneration of blocked active sites (PdS → PdO; $X_{O_2,0}$(T = 250 °C) = 0.2 → $X_{O_2,res}$ = 0.015 → oxygen consumption: 61 ppmv → n_{H_2S}: $n_{O_2} \approx 1{:}1$). After approximately three hours, a slight breakthrough of H_2S occurs in the off-gas ($y_{H_2S,out}$ = 10 ppmv) at T = 250 °C.

In contrast, when the deactivation experiment is carried out at 300 °C, a minor methane conversion still takes place even after 10 h. In addition, the decrease of activity is delayed for approximately 2 h, which is equivalent to the moment when a breakthrough of SO_2 of approximately 20 ppmv occurs in the off-gas. Until then, the complete amount of sulfur in the feed remains on the catalyst surface.

Examinations with an empty reactor (under the same operating conditions) indicate for some conversion of H_2S to SO_2 at higher temperatures, very likely catalyzed by the reactor itself ($X_{H_2S \rightarrow SO_2}$ (300 °C) = 40%). At 250 °C, however, no formation of SO_2 is observed.

Deactivation experiments in literature (under excess oxygen conditions) usually come to the conclusion that deactivation by H_2S or by SO_2 is equivalent for reasons already mentioned. Since this is not the case under this works operating conditions, the influences of both gases on catalyst deactivation have been examined separately.

4.1.2. Influence of sulfur dioxide on catalytic activity

Under typical excess oxygen conditions SO_2 leads to the formation of $PdSO_X$-species with no or only minor residual activity for methane oxidation [17,18]. To eliminate any influences of the applied reaction system, examinations under literature conditions (1,500 ppmv CH_4 in excess of O_2) have been carried out. A plot of X_{CH_4} vs. time is included in the Supplementary data section. In accordance to literature, under suchlike operating conditions SO_2 leads to a decrease in methane conversion. Additionally, a minor residual activity is confirmed [26].

Fig. 3 again shows the influence of SO_2 addition, but under oxygen removal conditions (= lower temperatures and methane in excess). Unexpectedly, under these conditions SO_2 leads to an increase of oxygen conversion, which is in average about 1.6 times higher compared to the standard degree of conversion ($X_{O_2,0}$) of a fresh catalyst. It appears as if any stable $PdSO_X$-intermediate with a higher activity than original PdO is formed. Furthermore, no deactivation at all is observed, even after 20 h TOS with 100 ppmv SO_2 in the feed gas.

For a reasonable explanation of the observed phenomena, the original reaction of oxygen with methane on PdO has to be taken into consideration. The catalytic conversion of oxygen on noble metal catalysts can be described by the Eley–Rideal-mechanism [37,38]. Eley–Rideal presumes oxygen to be present in excess at the active sites of the catalyst at any time. Validity of this mechanism was confirmed in [41] for very low oxygen partial pressures as used in this work. Thus the partial pressure of oxygen shows no influence on the rate of reaction ($r_{CH_4} \sim {p_{O_2}}^0$). Eley–Rideal further presumes methane to take part in the reaction directly from the gas phase or from a short-term adsorbed state on the catalytic surface. Hence, at moderate pressures, the oxidation reaction is usually modelled first order in methane ($r_{CH_4} \sim {p_{CH_4}}^1$).

This implicates any $PdSO_X$ species to have a positive effect on rather the activity of the catalyst itself or on the adsorption of methane on the catalyst surface. Further it seems that the reactive intermediate is not stable at high temperatures or/and when high contents of oxygen are present in the feed gas (see Fig. 3), indicating why suchlike results have not been published yet.

Obviously, the catalyst behaves different after SO_2-feed is terminated. At T = 240 °C and $y_{O_2,0}$ = 1,025 ppmv the $PdSO_X$-intermediate is stable. The slight increase of conversion probably occurs as some physisorbed SO_2, inhibiting the oxidation reaction of methane, is desorbed from the catalyst.

A totally different behavior is observed at T = 290 °C and $y_{O_2,0}$ = 4,100 ppmv. Under these conditions the catalytic activity decreases to its original level (of PdO) after termination of the SO_2 feed. During the entire experiment, no SO_2 is detected in the off gas, indicating storage of sulfur in the support of the catalyst as aluminum sulfate and subsequent transformation of the active sites

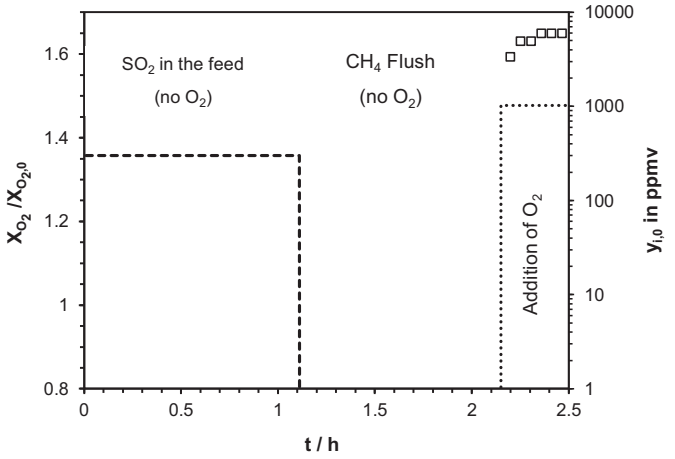

Fig. 4. Influence of oxygen on formation reaction of the $PdSO_X$-intermediate ($\dot{V}$ = 100 l/h (STP), $p_{CH_4,0}$ = 960 mbar, GHSV: 45,000 h^{-1}, p_{total} = 1.013 bar, T = 240 °C, balance: N_2): $X_{O_2}/X_{O_2,0}$ (□); $y_{O_2,0}$ (. . .); $y_{SO_2,0}$ (---).

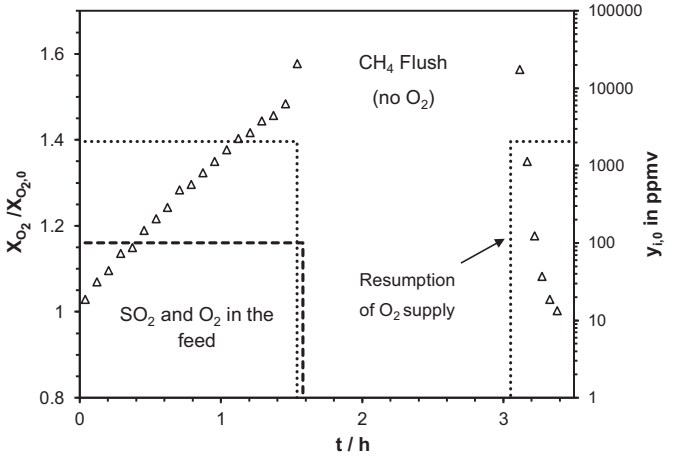

Fig. 5. Influence of oxygen on formation of PdO ($\dot{V}$ = 100 l/h (STP), $p_{CH_4,0}$ = 910 mbar, GHSV: 45,000 h^{-1}, p_{total} = 1.013 bar, T = 290 °C, balance: N_2): $X_{O_2}/X_{O_2,0}$ (Δ); $y_{O_2,0}$ (. . .); $y_{SO_2,0}$ (---).

back to PdO. This process probably also takes place during SO_2 feed, but the formation of the $PdSO_X$ intermediate however seems to be dominant at the reaction conditions applied.

4.1.3. Identification of reactive intermediate species

According to the literature, it is likely that the species with increased activity are either $PdSO_3$ [18] and/or $PdSO_4$ [17]. For further identification, the effect of oxygen on the formation of the $PdSO_X$-intermediate and its subsequent transformation to PdO was examined in detail. In order to confirm the experimental findings, X-ray fluorescence analysis (XRF) was also used.

Aforementioned examinations revealed that the active compound is stable at 240 °C and an oxygen inlet concentration of about 1,000 ppmv. Consequently, these conditions were used to examine the formation of the intermediate compound. Thus, the catalyst was exposed to SO_2 in an oxygen-free atmosphere where formation of palladium sulfite is expected (see Eq. (5)).

In order to prevent any inhibition of the combustion reaction (Eq. (1)) by adsorbed SO_2, the catalyst was flushed with pure methane for approximately one hour after the formation segment. Thereafter, oxygen was added to the feed gas—and an increased activity was apparent immediately. Consequently, it can be stated that oxygen is not necessary to form the active $PdSO_x$-intermediate, when SO_2 is applied. This finding indicates palladium sulfite ($PdSO_3$) or any compound with an equal Pd:O ratio to be the active intermediate. Fig. 4 illustrates the applied experimental procedure and the results.

To verify $PdSO_3$ as the active intermediate, the influence of oxygen during recovery of PdO was examined additionally. In contrast to $PdSO_4$, $PdSO_3$ requires oxygen to form $Al_2(SO_4)_3$ and restore PdO (Eq. (16)).

Upon this second attempt the $PdSO_x$ species was formed in a methane/sulfur dioxide (100 ppmv)/oxygen (4,100 ppmv) atmosphere at higher temperature. Fig. 5 shows the procedure. After terminating both, the SO_2 and O_2 feed, the reactor was again passed through an isothermal flush cycle at 290 °C for approximately 1.5 h. After resumption of oxygen supply, the conversion is apparent immediately, but a fast decrease of activity—back the original activity level of PdO—occurs. It can be therefore stated, that not only high temperatures but oxygen is needed for completing the regeneration cycle of the active compound. This again indicates for $PdSO_3$ as the active intermediate species.

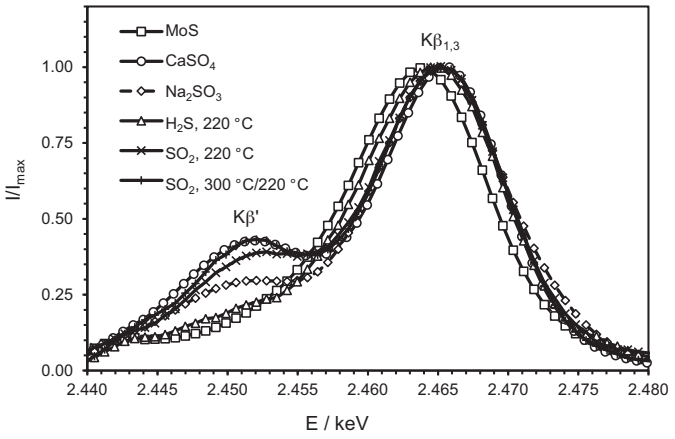

Fig. 6. Kβ′, $K\beta_{1,3}$—scan of Pd-Al_2O_3 catalyst spheres after reaction with H_2S at 220 °C, SO_2 at 220 °C and SO_2 at 300 °C/220 °C. MoS, Gypsum and Na_2SO_3 are given for comparison.

4.2. Results of XRF species analysis

For XRF analysis, three catalyst samples were prepared by applying different gaseous sulfur compounds and reaction temperatures: H_2S at 220 °C (→PdS), SO_2 at 220 °C (→$PdSO_3$) and one Pd-sample on Al_2O_3 carrier after exposure to SO_2 first at 300 °C followed by 220 °C (→$PdSO_3$→ + $Al_2(SO_4)_3$). Fig. 6 shows the resulting scans across the Kβ′ and $K\beta_{1,3}$-lines.

The $K\beta'/K\beta_{1,3}$ intensity ratio increases from 0.077 for the reaction with H_2S at 220 °C to 0.242 for the reaction with SO_2 starting at 300 °C and then decreasing to 220 °C. The ratio for the reaction with SO_2 at 220 °C is slightly lower but with 0.223 clearly higher than 0.143, the ratio of Na_2SO_3. Even after the reaction with H_2S a small Kβ′-peak is visible and the ratio (0.077) is slightly higher than that of MoS (0.023). A comparison of the $K\beta'/K\beta_{1,3}$ intensity ratios is given in Table 3.

The $K\beta'/K\beta_{1,3}$ intensity ratios imply, that after reaction with H_2S the sulfur is mainly bound as PdS. A small part seems to be present as $PdSO_3$ or $PdSO_4$. This may be caused by oxidation with O_2 from the air after the H_2S-reaction. This is supported by the fact, that the ratio increases if the same samples are measured after considerably longer contact with air (Fig. 7).

The $K\beta'/K\beta_{1,3}$ ratio of SO_2 at 220 °C is higher than the ratio of Na_2SO_3 and slightly lower than the $SrSO_4$ ratio. This implies that

Table 3
Kβ′/ $K\beta_{1,3}$ intensity ratio for the catalyst material after reaction with H_2S and SO_2 at different temperatures forming sulfides, sulfites and sulfates. The intensity ratio of S at the Kβ' position to the $K\beta_{1,3}$ intensity was set as zero point.

Preparation of catalyst samples for XRT / Compounds	Kβ′/$K\beta_{1,3}$ intensity ratio
Deactivation with 50 ppmv of H_2S at T = 220 °C	0.067
Application of 50 ppmv SO_2 at T = 220 °C	0.223
50 ppmv of SO_2 at 300 °C; SO_2 at 220 °C; SO_2 while cooling to RT	0.242
$CaSO_4$*$2H_2O$	0.278
Na_2SO_3	0.143
MoS	0.023
$SrSO_4$	0.269

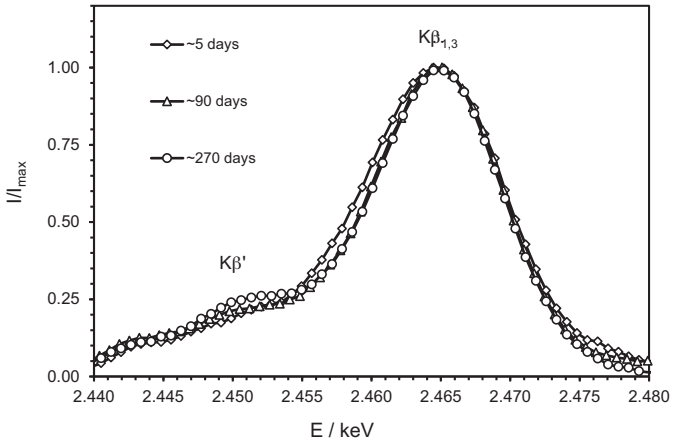

Fig. 7. Time dependency of the Kβ′/$K\beta_{1,3}$-ratio for the sample after reaction with H_2S at 220 °C.

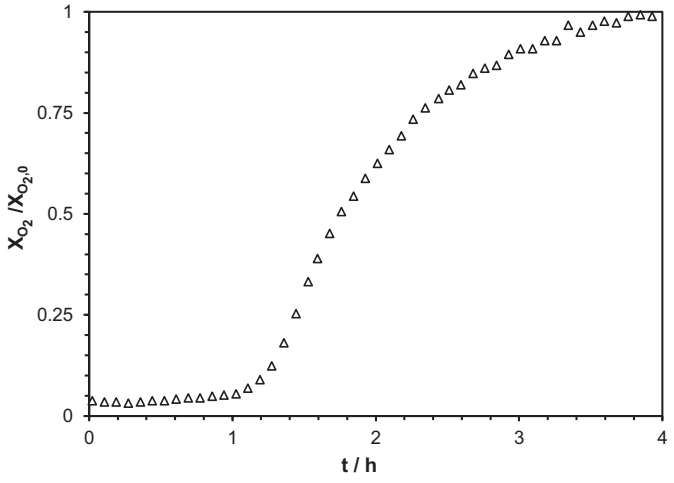

Fig. 8. In-situ regeneration of a deactivated PdO/Al_2O_3 catalyst after termination of H_2S-feed ($\dot{V}$ = 100 l/h (STP), $p_{CH4,0}$ = 960 mbar, $y_{O2,0}$ = 4,100 ppmv, GHSV: 45,000 h^{-1}, p_{total} = 1.013 bar, T = 296 °C, balance: N_2).

a small part is present as $PdSO_3$ and the major part as SO_4^{2-}—but probably as $Al_2(SO_4)_3$. It seems as if oxidation of $PdSO_3$ to $Al_2(SO_4)_3$ occurs even at 220 °C, but formation of $PdSO_3$ is probably faster than the consecutive reaction of $PdSO_3$ to $Al_2(SO_4)_3$. The Kβ′/$K\beta_{1,3}$ ratio for the reaction with SO_2 at 300 °C followed by 220 °C is higher than for the reaction at 220 °C, but still slightly lower than that of $SrSO_4$. This clearly shows, that the major part of sulfur is bound as SO_4^{2-}, most likely as $Al_2(SO_4)_3$. A small part still is present as $PdSO_3$. As the applied catalyst exhibits only 0.5 ma% of PdO, consequently the determined amount of $PdSO_3$ is smaller than that of SO_4-species for all relevant samples (Fig. 8).

The results of this work correlate with the proposed mechanism by Yu and Shaw [18]. The formation of $PdSO_4$, as suggested by other authors [19,26], was not confirmed under the operating conditions applied in this work (see Figs. 4 and 5). However, deviations concerning catalytic activity of the $PdSO_X$-species between this work and literature observations occurred (see Supplementary data, Fig. B vs. Figs. 3–5). One possible explanation could be that $PdSO_4$ (with low activity for oxidation of methane) might be formed when high oxygen contents are applied, whereas formation of the reactive $PdSO_3$-intermediate occurs when only little oxygen is available in the gas phase.

The influence of SO_2 on the catalytic activity is furthermore able to account for the initially described delay in conversion decrease at 300 °C (see Fig. 2). The formation of $PdSO_3$ is probably able to compensate the loss of activity by formation of PdS. The SO_2 breakthrough occurs due to competing adsorption of H_2S and SO_2. At high sulfur loadings of the surface, SO_2 adsorption decreases, therefore the deactivation of the catalyst by H_2S dominates.

4.2.1. In-situ regeneration of the catalyst

Finally, the regeneration of the deactivated catalyst was examined. Fig. 1 shows a characteristic regeneration curve after the H_2S exposure to the catalyst is terminated. Typically all samples for regeneration measurements were pre-treated with 100 ppmv of H_2S until residual activity for methane oxidation = 0.

Equivalent to the termination of the deactivation measurements, no CO_2 is detected at the beginning of the catalyst regeneration phase. After a delay of approximately one hour (in this case), the activity recovers in the course of the measurement back to its original level. No sulfur compounds are detected in the off-gas, indicating for storage of the complete sulfur loading in the catalyst support. Therefore it is very likely that palladium sulfide is oxidized to sulfite, followed by formation of $Al_2(SO_4)_3$ and recovery of PdO, equivalent to the measurements with SO_2.

The delay in regeneration is a consequence of excess of H_2S on the catalyst surface, which was adsorbed on the support during deactivation experiment. Under the assumption that the complete amount of palladium on the catalyst surface is accessible for H_2S and a 1:1 stoichiometry is valid for deactivation, only 1/11 of the amount of H_2S which is necessary to completely deactivate the catalyst reacts with the active compound. The rest is adsorbed on the support material (see Section 4.5.3, Figure 17). This excess of sulfur on the catalyst surface is very likely to re-cover the active sites after they are regenerated. After degradation of this sulfur reservoir, recovery of methane conversion becomes visible. In contrary to Ordonez et al. [28], a complete in-situ recovery of the catalytic activity under reaction conditions is possible, as the original activity of the fresh catalyst is reached. The experimental findings lead to the conclusion that the active compound is regenerated to PdO and that $Al_2(SO_4)_3$ neither physically blocks active sites nor significantly narrows pores at conditions applied in this work, which would lead to a mass transfer limitation of the methane oxidation. However, how many deactivation and regeneration cycles are possible with one catalyst has not been determined in this work, as for all experiments, a fresh catalyst was used.

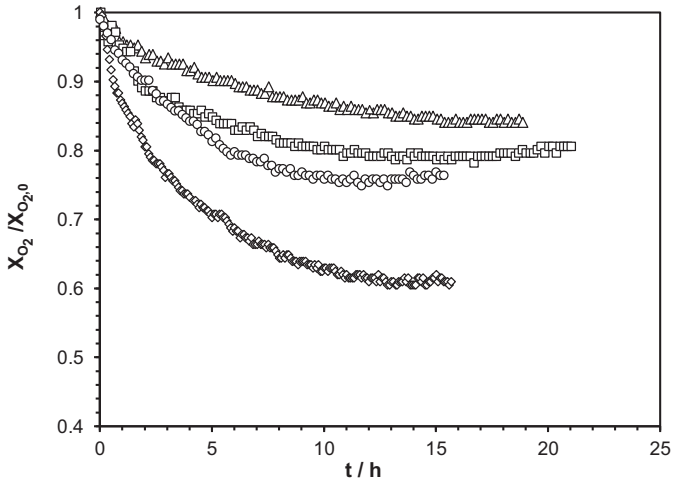

Fig. 9. Influence of low $p_{H_2S,0}$ on the oxygen conversion ($\dot{V}$ = 100 l/h (STP), $p_{CH_4,0}$ = 960 mbar, $y_{O_2,0}$ = 4,100 ppmv, GHSV: 45,000 h^{-1}, p_{total} = 1.013 bar, T = 280 °C, balance: N_2): $y_{H_2S,0}$ = 4 ppmv (Δ); $y_{H_2S,0}$ = 8 ppmv (□); $y_{H_2S,0}$ = 10 ppmv (○); $y_{H_2S,0}$ = 14 ppmv (◊).

4.3. Reaction scheme

When high partial pressures of H_2S (≥20 ppmv) are used for the deactivation experiments, the in-situ regeneration reactions are obviously too slow for achieving a stationary state on the catalyst surface. But, when low partial pressures of the catalyst poison are applied, e.g. in the case where the reaction is used for oxygen removal from fuel gas streams, an equilibrium state between deactivation and regeneration is expected, probably leading to the residual activities observed by some authors [8,25,26]. In such a case, different states of the active compound (Pd) are likely to be present on the catalyst surface, whereby the ratios of PdO, PdS and $PdSO_3$ depend on the applied reaction conditions (T, p_i).

In order to verify this assumption, measurements with low partial pressures of hydrogen sulfide were carried out. The reaction temperature was chosen as high as possible for fast in-situ regeneration of the catalyst, but low enough for minor H_2S conversion to SO_2 in the gas phase. The results for four different partial pressures of H_2S at 280 °C are shown in Fig. 9.

As can be seen, constant and comparably high residual activities are achieved for each of the examined partial pressures. An increase of H_2S content leads to lower residual activities due to intensification of deactivation. These results are in contrast to Ordonez et al. [26], who observed one single residual activity, which was independent of the partial pressure of the catalyst poison.

It could be that the regeneration of PdO from $PdSO_4$ (presumed to be present at high oxygen contents) is slower than the regeneration from $PdSO_3$ to PdO (at low oxygen contents), leading to a high fraction of $PdSO_4$ on the catalytic surface under typical literature operating conditions. This may cause the single constant residual activity, observed by Ordonez et al. [26] even for different concentrations of H_2S. For deeper insights, additional experiments and sample analysis are necessary.

Based on the presented experimental findings, Fig. 10 gives a summary of the proposed reaction scheme for deactivation and regeneration of the PdO/Al_2O_3 catalyst, when low ratios of O_2:CH_4 are applied.

$$PdO + H_2S \rightarrow PdS\,(+H_2O) \quad (13)$$

$$PdS + 1.5O_2 \rightarrow PdSO_3 \quad (14)$$

$$PdO + SO_2 \rightarrow PdSO_3 \quad (15)$$

$$3PdSO_3 + 1.5O_2 + Al_2O_3 \rightarrow 3PdO + 3Al_2(SO_4)_3 \quad (16)$$

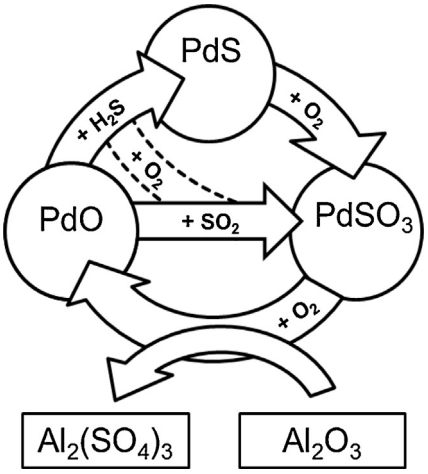

Fig. 10. Proposed deactivation and regeneration scheme of the PdO/Al_2O_3 catalyst for low O_2:CH_4 ratios.

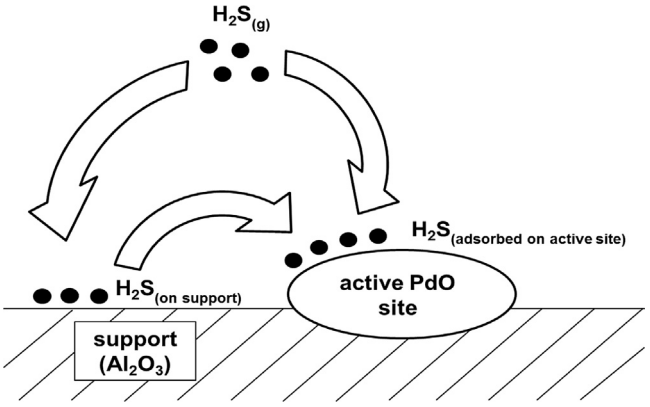

Fig. 11. PdS formation scheme.

4.4. Surface species modelling

In order to describe temporal changes of catalyst activity, Levenspiel [39] proposed an empirical model consisting of a deactivation function Ψ, depending on the temperature and the partial pressure of the catalyst poison p_i and a deactivation order d on the original catalyst activity a (Eq. (17)).

$$-\frac{da}{dt} = \Psi(p_i, T) * a^d \quad (17)$$

In an advanced version, the model was adapted to account for residual activities a_s (Eq. (18)).

$$-\frac{da}{dt} = \Psi(p_i, T) * (a - a_s(p_i, T))^d \quad (18)$$

Based on the approach of Froment [40], Ordonez et al. [26] proposed a different model for the catalytic oxidation of methane by PdO and the deactivation by sulfur which takes into account surface phenomena on the catalyst. Ordonez et al. assume that an active site of the catalyst can be present as palladium oxide (PdO) or as palladium sulfate ($PdSO_4$). Φ_{PdSO_4} represents the coverage fraction of $PdSO_4$ of all active sites. On the fresh catalyst, only PdO is present (Φ_{PdSO_4} = 0), whereby only $PdSO_4$ is existent on the completely deactivated catalyst (Φ_{PdSO_4} = 1). Eq. (19) shows Ordonez reaction rate approach. k_1 is the reaction constant of PdO, k_2 of $PdSO_4$.

$$-r_{O_2} = k_1 * \left(1 - \Phi_{PdSO_4}\right) * p_{CH_4} + k_2 * \Phi_{PdSO_4} * p_{CH_4} \quad (19)$$

The fraction of deactivated active sites can be described by Eq. (20), whereby k_s represents the deactivation constant and p_s the partial pressure of the catalyst poison.

$$\frac{d\Phi_{PdSO_4}}{dt} = k_s T * 1 - \Phi_{PdSO_4}{}^{n} * p_s^m \tag{20}$$

With this approach, Ordonez et al. [26] were able to describe the catalyst deactivation for different temperatures and partial pressures of SO_2. The surface species model proposed in this work is based on the approach of Ordonez et al. According to the experimental results at low O_2 partial pressures, the states of the active sites of the catalyst can rather be PdO, PdS or $PdSO_3$ (Eq. (21)).

$$\Phi_{PdO} + \Phi_{PdS} + \Phi_{PdSO_3} = 1 \tag{21}$$

The rate of total oxygen conversion is a result of the respective activity of the three possible states of the active compound (Eq. (22)).

$$r_{O_2} = \Phi_{PdO} * r_{O_2,PdO} + \Phi_{PdS} * r_{O_2,PdS} + \Phi_{PdSO_3} * r_{O_2,PdSO_3} \tag{22}$$

If possible, the reaction rates are related to the original reaction rate equation for methane oxidation (Eq. (23)) taken from [41] with kinetic parameters for PdO ($k_{0,CH_4-ox} = 1.1 \times 10^8$; $E_A = 87.8$ kJ/mol; B = 1.3; C = 2.5; D = 0.5; $K_{CO_2} = 1\ bar^{-2.5}$; $K_{H_2O,0} = 1.17 \times 10^{-5}\ bar^{-0.5}$; $\Delta_{ads}H_{H_2O} = 58.4$ kJ/mol).

$$-r_{O_2,i} = -a_i * r_{O_2,PdO} = k_{O_2} \cdot p_{CH_4}^B \cdot \frac{1}{(1 + K_{CO_2} p_{CO_2}^{2,5} + K_{H_2O} \cdot p_{H_2O}^{0,5})} \tag{23}$$

The calculations are carried out by a time discretized numerical method. The ratio $\Phi_{i,j}$ of the surface species i at time j are calculated on basis of the ratio $\Phi_{i,j-1}$ of the previous time step and its time discrete change (Eq. (24)).

$$\Phi_{i,j} = \Phi_{i,j-1} + \Delta t * \frac{d\Phi_{i,j-1}}{dt} \tag{24}$$

This leads to the calculation rules Eqs. (25)–(27) for the three possible states of the active compound palladium:

$$\Phi_{PdS,j} = \Phi_{PdS,j-1} + \Delta t * \left(\left(\frac{d\Phi_{PdS,j-1}}{dt} \right)_{PdO \to PdS} - \left(\frac{d\Phi_{PdS,j-1}}{dt} \right)_{PdS \to PdSO_3} \right) \tag{25}$$

$$\Phi_{PdSO_3,j} = \Phi_{PdSO_3,j-1} + \Delta t * \left(\left(\frac{d\Phi_{PdSO_3,j-1}}{dt} \right)_{PdS \to PdSO_3} - \left(\frac{d\Phi_{PdSO_3,j-1}}{dt} \right)_{PdSO_3 \to PdO} \right) \tag{26}$$

$$\Phi_{PdO,j} = \Phi_{PdO,j-1} + \Delta t * \left(\left(\frac{d\Phi_{PdO,j-1}}{dt} \right)_{PdSO_3 \to PdO} - \left(\frac{d\Phi_{PdO,j-1}}{dt} \right)_{PdO \to PdS} \right) \tag{27}$$

The formation of PdO out of PdS is described by rate Eq. (28). An oxygen dependency is considered, see Eq. (16).

$$\frac{d\Phi_{PdO}}{dt} = k_{PdO}(T) * \Phi_{PdSO_3}^{n_{PdO}} * p_{O_2}^{m_{PdO}} \tag{28}$$

A similar approach is used to describe the formation of $PdSO_3$ by oxidation of PdS (Eq. (29)).

$$\frac{d\Phi_{PdSO_3}}{dt} = k_{PdSO_3}(T) * \Phi_{PdS}^{n_{PdSO_3}} * p_{O_2}^{m_{PdSO_3}} \tag{29}$$

Again, oxygen partial pressure is taken into consideration, see Eq. (14).

As already mentioned, the formation of PdS from PdO and H_2S occurs by two different routes and thus a different modelling approach must be applied. With a fresh catalyst, for the first minutes of the deactivation experiment, the formation of PdS mainly results from direct adsorption of H_2S from the gas phase on the active sites, followed by the deactivation reaction (Eq. (2)). But H_2S also adsorbs on the catalyst support, leading to an increase in sulfur loading of the Al_2O_3 surface during the experiment (see Fig. 11). As already shown during regeneration measurements, this sulfur sink is not inert throughout the reaction cycle. During deactivation measurements it additionally re-occupies free and/or already regenerated active sites. Therefore, some assumptions for modelling of the deactivation process have to be applied.

This leads to the following approach to describe the formation of PdS from PdO (Eq. (30)):

$$\left(\frac{d\Phi_{PdS}}{dt} \right)_{PdO \to PdS} = \left(\frac{d\Phi_{PdS}}{dt} \right)_{from\ gas\ phase} + \left(\frac{d\Phi_{PdS}}{dt} \right)_{from\ support} \tag{30}$$

The formation of PdS directly from the gas phase shows a dependency of partial pressure of H_2S and of PdO-ratio. For modelling of the reaction a rate constant k_{PdS} is applied (Eq. (31)).

$$\frac{d\Phi_{PdS}}{dt}_{from\ gas\ phase} = k_{PdS} * p_{H_2S}^{m_{PdS}} * \Phi_{PdO}^{n_{PdS}} \tag{31}$$

The formation of PdS from surface H_2S is modelled by a sulfur surface diffusion term, incorporating the fraction of PdO and the sulfur coverage θ of the support, representing the driving force for mass transfer (Eq. (32)).

$$\frac{d\Phi_{PdS}}{dt}_{from\ support} = k_\Theta * \Theta * \Phi_{PdO}^{n_\Theta} \tag{32}$$

The sulfur coverage θ of the support is defined by the ratio of the accumulated sulfur loading $N_S(t)$ and the maximum possible sulfur loading $N_{S,max}$ (Eq. (33)).

$$\Theta = \frac{N_S(t)}{N_{S,max}} \tag{33}$$

Since $N_{S,max}$ is not easily accessible, a new rate constant k′ is defined (Eq. (34)):

$$k' = \frac{k_\Theta}{N_{S,max}} \tag{34}$$

The change in sulfur loading is defined by the remaining amount of H_2S that is stored in the packing less the PdS formation reactions (Eq. (35)).

$$\left(\frac{dN_{s,j^{-1}}}{dt} \right) = \dot{N}_{H_2S,in} - \dot{N}_{H_2S,out} - \dot{N}_{PdO} * \left(\left(\frac{d\Phi_{PdS,j^{-1}}}{dt} \right)_{gas\ phase} + \left(\frac{d\Phi_{PdS,j^{-1}}}{dt} \right)_{support} \right) \tag{35}$$

In the context of this work, it is assumed that all PdO atoms are accessible on the catalyst surface and that each PdO reacts with one H_2S molecule.

4.5. Examinations on reaction kinetics

As any $PdSO_3$ or equivalent component is metastable under at least some of the applied reaction conditions, it was possible to carry out separate kinetic studies on the most important reactions of the proposed reaction scheme (Section 4.5.1–4.5.3).

4.5.1. Regeneration of PdO from $PdSO_3$

The experimental procedure for determination of regeneration kinetics of PdO is similar to the procedure applied in Fig. 5. $PdSO_3$ was formed under an SO_2 and O_2 containing atmosphere and afterwards the catalyst was flushed with methane. The conversion of oxygen was monitored after oxygen feed was re-enabled after the flush cycle. Despite the high reaction rates($r_{O_2,PdSO_3} = 1.6\ \ r_{O_2,PdO}$),

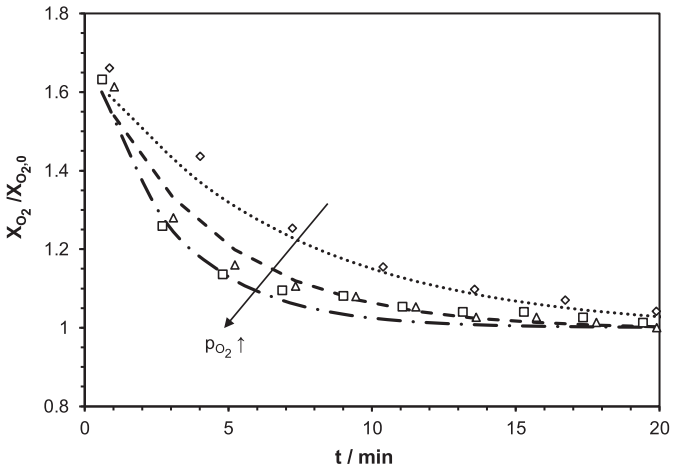

Fig. 12. Influence of p_{O_2} on the regeneration reaction of PdO from $PdSO_3$ ($\dot{V}$ = 100 l/h (STP), $p_{CH_4,0}$ = 910 mbar, T = 250 °C, GHSV: 45,000 h^{-1}, p_{total} = 1.013 bar, balance: N_2): $y_{O_2,0}$ = 2,050 ppmv: exp (◊), calc (. . .); $y_{O_2,0}$ = 3,075 ppmv: exp(Δ), calc (---); $y_{O_2,0}$ = 4,100 ppmv: exp (□), calc (▬ ▪).

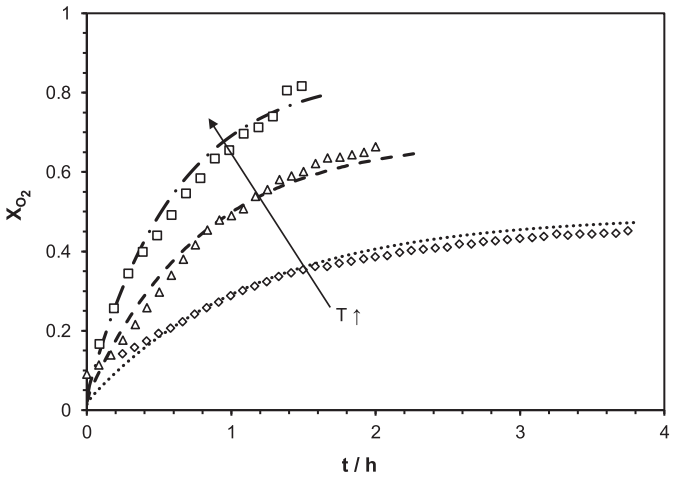

Fig. 14. Temperature influence on the PdO-formation from PdS and comparison of experimental results and calculated conversion for the formation of PdO from PdS at different temperatures ($\dot{V}$ = 100 l/h (STP), $p_{CH_4,0}$ = 960 mbar, $y_{O_2,0}$ = 4,100 ppmv, GHSV: 45,000 h^{-1}, p_{total} = 1.013 bar, balance: N_2): T = 277 °C: exp (◊), calc (. . .); T = 288 °C: exp(Δ), calc (---); T = 296 °C: exp (□), calc (▬ ▪).

it was possible to determine the influences of oxygen partial pressure and temperature on the reaction $PdSO_3 \rightarrow PdO$ (Eq. (16)). As can be seen in Figs. 12 and 13 an increase in oxygen partial pressure and temperature both result in faster PdO formation, which is typical for an oxidation reaction.

The regeneration reaction of PdO from $PdSO_3$ can be divided into three consecutive steps:

a. Oxidation of SO_2, which is chemically bound on PdO, to (PdO-)SO_3
b. Transport (by surface diffusion) of SO_3 to the surrounding Al_2O_3 surface
c. Storage of SO_3 as $Al_2(SO_4)_3$ in the catalyst support

The positive effect on the regeneration rate by an increase in oxygen content in the feed gas leads to the conclusion that step (a) is the rate-determining step, as the consecutive transport step should exhibit no oxygen dependency.

Finally the kinetic parameters for this reaction were evaluated. For the measurements, it was assumed, that at the beginning of the experiment the active sites are present exclusively as $PdSO_3$ (Φ_{PdSO_3} = 1) and at the end of regeneration, total conversion to PdO (Φ_{PdO} = 1) has occurred. Fig. 12 shows furthermore a comparison of the experimental data and the calculation results for different partial pressures of oxygen. Both, the temperature and oxygen dependence can be described satisfactorily with the parameters in Table 4.

Further, it can be assumed that when high surface coverage of the support material with e.g. H_2S or water occurs, the oxidation reaction of $PdSO_3$ and furthermore the surface diffusion process could be inhibited [19]. However, such conditions were not applied in this study.

4.5.2. Formation of PdO from PdS

As the kinetics of the $PdSO_3 \rightarrow PdO$ reaction are established, it is possible to access the kinetic parameters of the previous formation reaction of $PdSO_3$ from PdS. Fig. 14 shows the normalized oxygen conversion progression of a completely deactivated catalyst, some time period after the termination of the H_2S pretreatment (100 ppmv of H_2S until residual activity for methane oxidation = 0) for three different reaction temperatures. As can be

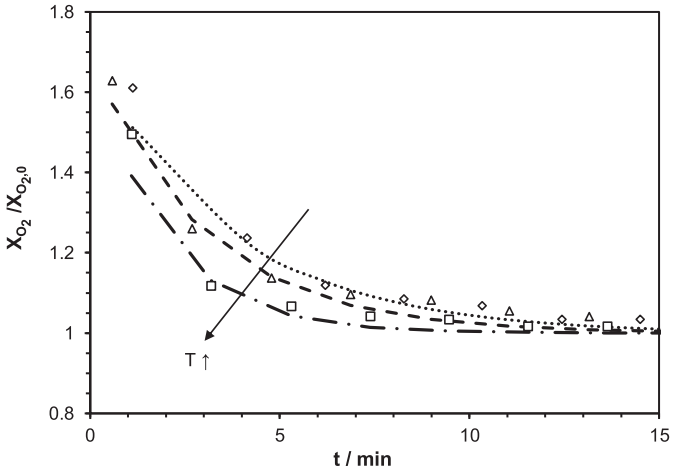

Fig. 13. Influence of temperature on the regeneration reaction of PdO from $PdSO_3$ ($\dot{V}$ = 100 l/h (STP), $p_{CH_4,0}$ = 910 mbar, $y_{O_2,0}$ = 4,100 ppmv, GHSV: 45,000 h^{-1}, p_{total} = 1.013 bar, balance: N_2): T = 240 °C: exp (◊), calc (. . .); T = 250 °C: exp (Δ), calc (---); T = 265 °C: exp (□), calc (▬ ▪).

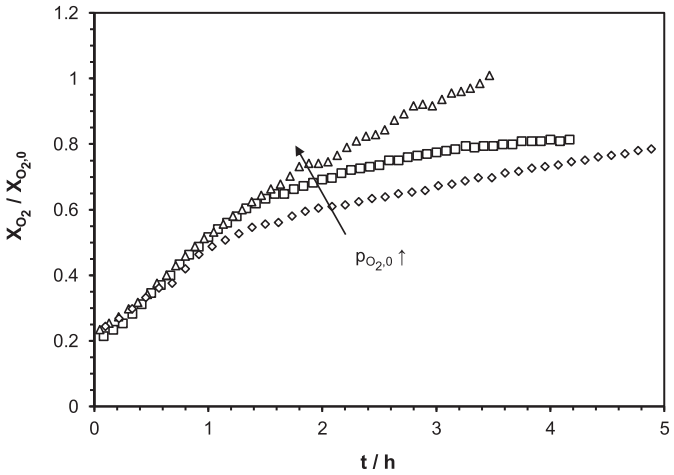

Fig. 15. Influence of p_{O_2} on the formation of PdO from PdS ($\dot{V}$ = 100 l/h (STP), $p_{CH_4,0}$ = 960 mbar, T = 277 °C, GHSV: 45,000 h^{-1}, p_{total} = 1.013 bar, balance: N_2): $p_{O_2,0}$ = 4 mbar (□), 3 mbar (Δ) and 2 mbar (◊).

Table 4
Kinetic parameters of the reactions involved in the proposed reaction scheme, see Fig. 10.

Reaction	Parameter	$k_{0,i}$	E_A	m_i	n_i	k'	n_θ	Eq.
$PdSO_3$ to PdO	Unit	h^{-1} bar^{-m}	kJ/mol	-	-	h^{-1}	–	–
	Value	2.6×10^{10}	60.5	1.25	1	–	–	(28)
PdS to $PdSO_3$	Unit	h^{-1}	kJ/mol	-	-	–	–	–
	Value	1.6×10^{7}	74	0	1.35	–	–	(29)
PdS formation	Unit	h^{-1} bar^{-m}	kJ/mol	-	-	h^{-1}	–	–
	Value	1.1×10^{4}	74	1	1.3	4.5	0.1	(31), (32)

seen, an increase in temperature promotes the regeneration of the catalyst (Fig. 15).

For analysis of the regeneration curves, an idle time segment at the beginning of the experiments (see Fig. 1) is neglected, as the elimination of surface sulfur does not cause an increase in oxygen conversion (due to re-coverage of active sites). Only when the amount of active sulfur on the surface is fairly eliminated, the regeneration of the catalyst gets visible by an increase of oxygen conversion (due to oxidation of methane at the regenerated PdO sites).

As already noted, the regeneration of PdS consists of two reaction steps, the oxidation of PdS to $PdSO_3$ and the consecutive recovery of PdO under formation of $Al_2(SO_4)_3$. Comparison of the time scale of both reactions (Figs. 12 and 14) leads to the conclusion that the oxidation of PdS is the rate-determining step in the reaction scheme. $PdSO_3$ is a metastable intermediate species—at temperatures above 250 °C its retention time on the catalyst surface is short, therefore the ratio of $PdSO_3$ on the surface tends to be fairly small ($\Phi_{PdSO_3} \rightarrow 0$).

Furthermore, the influence of the oxygen partial pressure was examined. As can be seen, in the first hour of measurements, regeneration rates equal each other. Therefore, it seems as if the partial pressure of oxygen had no influence on the regeneration of active sites (when at least 2,000 ppmv of oxygen are applied to the feedgas). After approximately one hour a decrease of reaction rate occurs with the lowest of the applied inlet concentrations of oxygen. Most likely, the active sites in the upper part of the catalyst bed are then regenerated. As a consequence a depletion of oxygen occurs in the lower region of the bed due to recoverage of methane combustion in the upper part. Thus p_{O_2} decreases in the lower part of the bed, resulting in an inhibition of the regeneration reaction. Nevertheless, in a technical application the strongest sulfur loading is expected at the top part of the catalyst bed, especially in continuous operation mode. Simultaneously, this is where the oxygen content is highest. Thus an influence of oxygen on the regeneration of deactivated palladium sites is neglected. Finally the kinetic parameters for the oxidation of PdS to $PdSO_3$ (Eq. (31)) were determined (see Table 4). The results of the fits are shown in Fig. 14. As can be seen, the calculated conversion rates are in good agreement with the experimental results.

4.5.3. Deactivation of PdO by formation of PdS

Fig. 16 shows the decrease of oxygen conversion with different concentrations of hydrogen sulfide (GHSV of 45,000 h^{-1}) with a constant temperature and besides H_2S an equal gas composition. It is apparent that an increase of partial pressure of H_2S results in an intensification of catalyst deactivation.

Furthermore, Fig. 17 shows the oxygen conversion as a function of accumulation of H_2S ($n_{H_2S,total}/n_{PdO,catalyst}$) on the catalyst surface. Since the amount of H_2S for a complete deactivation of the catalyst is almost equal for different partial pressures of H_2S, the total injected quantity of H_2S, not its partial pressure, is the most important factor for the deactivation of the catalyst.

Besides, if sulfur deposited at the active sites primarily, a complete deactivation of the catalyst would occur at a specific amount of H_2S of one (under the assumption that all PdO molecules are

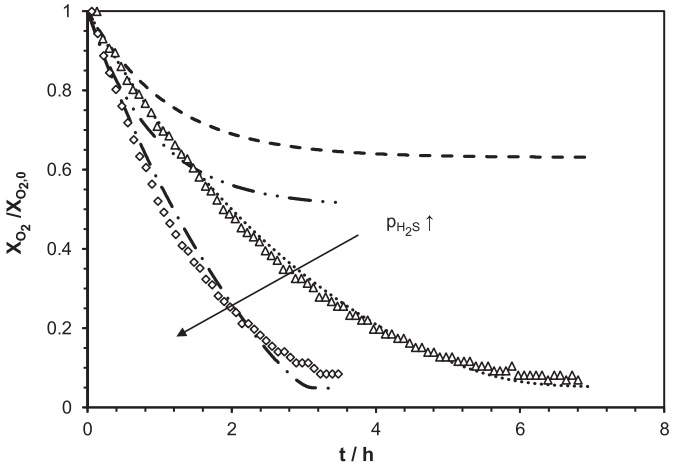

Fig. 16. Comparison between experimental and calculated data for the deactivation at different partial pressures of H_2S ($\dot{V}$ = 100 l/h (STP), $p_{CH_4,0}$ = 960 mbar, GHSV: 45,000 h^{-1}, p_{total} = 1.013 bar, $y_{O_2,0}$ = 2,050 ppmv, T = 250 °C, balance: N_2): $y_{H_2S,0}$ = 50 ppmv: exp (◊), calc without support-sulfur (▬ . .), calc with support-sulfur (▬ . .); $y_{H_2S,0}$ = 30 ppmv: exp (Δ), calc without support-sulfur (---), calc with support-sulfur (. . .).

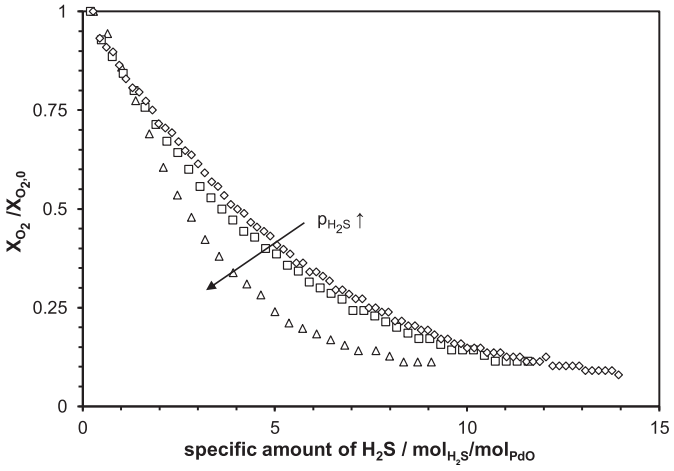

Fig. 17. Influence of p_{H_2S} as a function of the specific amount of H_2S per moles of PdO ($\dot{V}$ = 100 l/h (STP), $p_{CH_4,0}$ = 960 mbar, GHSV: 45,000 h^{-1}, p_{total} = 1.013 bar, $y_{O_2,0}$ = 2,050 ppmv, T = 250 °C, balance: N_2): $y_{H_2S,0}$ = 100 ppmv (Δ), 50 ppmv (□), 30 ppmv (◊).

accessible on the catalyst surface and that one PdO site reacts with one single H_2S molecule). However, the experimental results indicate that the major part of H_2S adsorbs on the support, not at the active sites. Still, no sulfur desorption occurs after terminating the H_2S feed, indicating for an additional strong chemisorption of H_2S on the catalyst support.

Fig. 18 shows the influence of p_{O_2} on the formation of PdS from PdO. The deactivation rates do not deviate significantly in the first (two) hours of the experiments. Thereafter, the conversion of oxygen at 1,025 ppmv decreases faster. This is probably an

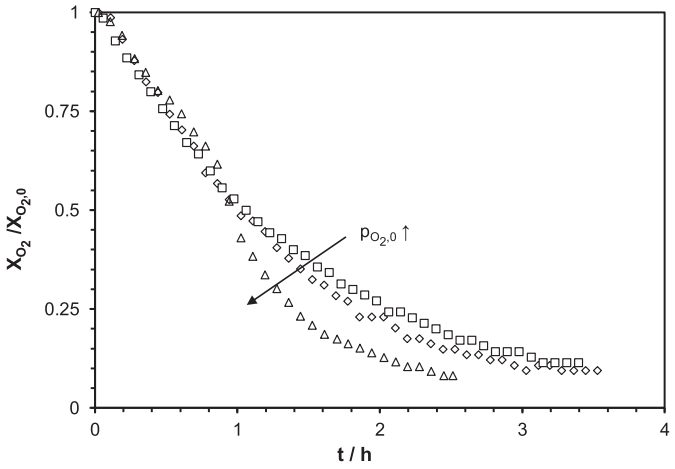

Fig. 18. Influence of p_{O_2} on the formation of PdS from PdO ($\dot{V}$ = 100 l/h (STP), $p_{CH_4,0}$ = 960 mbar, GHSV: 45,000 h^{-1}, p_{total} = 1.013 bar, $y_{H_2S,0}$ = 50 ppmv, T = 250 °C, balance: N_2): $y_{O_2,0}$ = 1,025 ppmv (Δ), 2,050 ppmv (□), 4,100 ppmv (◊).

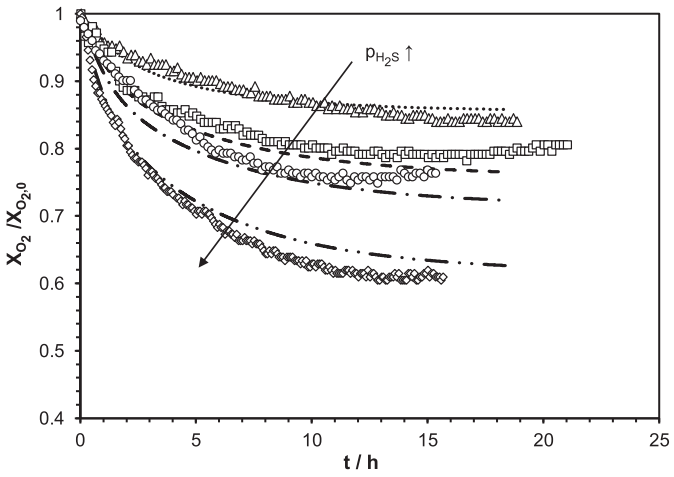

Fig. 19. Comparison between experimental and calculated data for catalyst deactivation at different partial pressures of H_2S ($\dot{V}$ = 100 l/h (STP), $p_{CH_4,0}$ = 960 mbar, GHSV: 45,000 h^{-1}, p_{total} = 1.013 bar, $y_{O_2,0}$ = 4,100 ppmv, T = 280 °C, balance: N_2): $y_{H_2S,0}$ = 14 ppmv: exp (◊), calc (▬ ▪ ▪); $y_{H_2S,0}$ = 10 ppmv: exp (○), calc (▬ ▪); $y_{H_2S,0}$ = 8 ppmv: exp (□), calc (---); $y_{H_2S,0}$ = 4 ppmv: exp (Δ), calc (. . .).

effect of pore-narrowing leading to a mass transfer limitation of the methane oxidation and/or the regeneration reaction of PdS, caused by depletion of oxygen at the inner active sites. Indeed, this phenomenon does not occur at higher partial pressures of oxygen. Thus, as expected from reaction stoichiometry, it is assumed that p_{O2} has no significant influence on the formation of PdS.

Furthermore the influence of temperature was examined. The applicable temperature range for the measurements is limited by SO_2 formation (280 °C) and by the minimum temperature for oxygen conversion (235 °C). A temperature effect on deactivation reaction is not visible within these boundaries. In literature, adsorption of sulfur, not the consecutive reaction with the active compound is considered to be the rate-determining reaction step [17,25]. Probably due to the small variation range, changes of temperature show no effect on sulfur adsorption. At the end of the experiments no activity for methane oxidation is observed anymore($r_{O_2,PdS} = 0$), additionally a minor H_2S breakthrough appears. Higher reaction temperatures result in a slight increase of residual activities, which is not due to higher activity for oxidation of methane but due to an increase of regeneration rate.

Finally, the kinetic parameters for the formation of PdS were derived. As already addressed, the formation of PdS occurs directly by H_2S adsorption on the active sites but additionally by surface diffusion of sulfur molecules, adsorbed on the catalyst support. The deactivation directly from the gas phase was adapted to the initial degradation rate (slope of the deactivation curves within the first minutes of measurements), as it is assumed that the amount of sulfur on the support (and therefore the formation of PdS from support-sulfur) is low in this time period. As deactivation progresses, more and more support-sulfur takes part and additionally covers the active sites. The kinetic parameters of this term are predominantly fitted to the end of the deactivation measurements. The derived parameters are summarized in Table 4. Fig. 16 shows the experimental results and calculated conversion rates for 30 ppmv and 50 ppmv of H_2S at low temperatures. For demonstration, the conversion rates are calculated with and without PdS-formation from support-sulfur.

To summarize the results, Fig. 19 shows the measurements at low feed concentrations of H_2S, which result in residual activities, as deactivation and regeneration rates equal each other. As can be seen, it is possible to calculate the residual activities, when the kinetic parameters of the involved reactions are incorporated, which were derived from separate experimental studies on each reaction. Fig. 20 shows a parity plot of all experimental vs. calculated data.

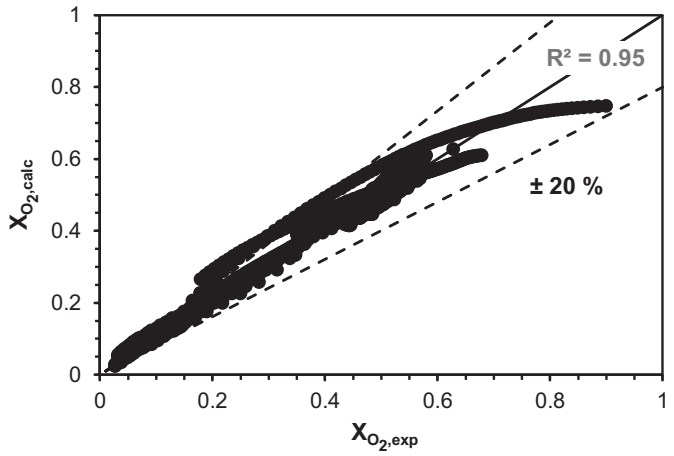

Fig. 20. Parity Plot of experimental oxygen conversion vs. model prediction.

5. Summary and conclusion

As sulfur compounds are important gas contaminants in the gas industry, this work focuses on the effect of sulfur-containing gas components on the durability of a commercial PdO/Al_2O_3 catalyst for removal of oxygen by oxidation of CH_4 at low O_2:CH_4 ratios, an operating temperature range of 200 °C < T < 300 °C and low H_2S contents.

As SO_2 and H_2S show a different behavior in the examined range of operating conditions, the influences of both were determined separately in course of preliminary examinations on catalyst deactivation and consecutive in-situ regeneration. Due to the low operating temperatures and low oxygen contents applied in this work, it was possible to identify an intermediate species, presumably $PdSO_3$, with an increased activity for the oxidation of methane. This stands in contrast to the literature, where SO_2 typically causes catalyst deactivation. As a conclusion, it can be drawn that oxygen content in the gas phase may have an influence on oxidation stage of the $PdSO_X$ component spectrum on the catalyst surface. Based on the experimental results, a reaction scheme was derived and

kinetic measurements for each of the participating reactions were carried out separately.

Furthermore, the derived deactivation model was validated by experimental data with low contents of H_2S, showing that the residual activities, observed by some authors, are a result of rate-equality of deactivation and in-situ regeneration process on the catalytic surface.

In further investigations, more detailed information on catalyst surface species can be obtained by using extended X-ray absorption spectroscopy (EXAFS) at an adequate synchrotron beamline. EXAFS enables the determination of the atomic environment as well of the Pd-atoms as of the sulfur atoms.

The results of this work are useful in particular when low contents of H_2S or SO_2 (<1–2 ppmv) are applied to the catalyst, e.g. in terms of oxygen removal with in-situ fine purification of the gas. Further on, first long-term deactivation measurements with high amounts of H_2S (which were not part of this work) reveal that a steady decline of conversion takes place after a certain TOS (depending on total H_2S amount applied to the catalyst). Whether the pores of the catalyst are physically blocked by surface sulfur, swelling of the support by storage of sulfate or other mechanisms take place has to be examined further, but passing through this type of deactivation is again fully reversible for the first few cycles. However, in order to deal with high H_2S amounts, it needs to be further examined how the long-term stability evolves, how many deactivation and regeneration cycles are possible until the catalyst support is completely saturated and irreversible deactivation takes place, respectively.

Acknowledgement

The authors are thankful for the funding from DVGW (German Technical and Scientific Association for Gas and Water).

Appendix A. Supplementary data

Supplementary data associated with this article can be found, in the online version, at http://dx.doi.org/10.1016/j.apcatb.2015.09.026.

References

[1] T. Muschalle, Influence of oxygen impurities on underground gas storage and surface equipment: Literature study, DGMK, Hamburg, 2013.
[2] DVGW e.V., G260 Gasbeschaffenheit, 2013.
[3] DVGW e.V., G 262 Nutzung von Gasen aus regenerativen Quellen in der öffentlichen Gasversorgung, 2011.
[4] EASEE-Gas, CBP. 2005-001/02: Harmonisation of Natural Gas Quality, 2005.
[5] B.H. Engler, Katalysatoren für den Umweltschutz, Chem. Ing. Tech. 63 (1991) 298–312.
[6] J.N. Armor, Energy efficiency and the environment: opportunities for catalysis, Appl. Catal. A 194–195 (2000) 3–11.
[7] T.R. Baldwin, R. Burch, Catalytic combustion of methane over supported palladium catalysts: I. alumina supported catalysts, Appl. Catal. 66 (1990) 337–358.
[8] P. Hurtado, S. Ordóñez, A. Vega, F.V. Díez, Catalytic combustion of methane over commercial catalysts in presence of ammonia and hydrogen sulphide, Chemosphere 55 (2004) 681–689.
[9] T.F. Garetto, C.R. Apesteguía, Oxidative catalytic removal of hydrocarbons over Pt/Al_2O_3 catalysts, Catal. Today 62 (2000) 189–199.
[10] J.M. Jones, V.A. Dupont, R. Brydson, D.J. Fullerton, N.S. Nasri, A.B. Ross, A.V.K. Westwood, Sulphur poisoning and regeneration of precious metal catalysed methane combustion, Catal. Today 81 (2003) 589–601.
[11] W. Köppel, F. Ortloff, R. Erler, G. Frank, Vermeidung und Entfernung von Sauerstoff bei der Einspeisung von Biogas in das Erdgasnetz, Abschlussbericht DVGW-Forschungsvorhaben G-1-05-10 (2010).
[12] F. Ortloff, F. Graf, T. Kolb, Ensuring operational safety of the natural gas grid by removal of oxygen from biogas via catalytic oxidation of methane, gas for energy, 2013, 58–65.
[13] S.J. Gentry, A. Jones, Poisoning and inhibition of catalytic oxidations: I. the effect of silicone vapour on the gas-phase oxidations of methane, propene, carbon monoxide and hydrogen over platinum and palladium catalysts, J. Chem. Technol. Biotechnol. 28 (1978) 727–732.
[14] R. Auer, M. Alifanti, B. Delmon, C.T. Fernand, Catalytic combustion of methane in the presence of organic and inorganic compounds over $La_{0.9}Ce_{0.9}Ce_{0.1}CoO_3$ catalyst, Appl. Catal. B 39 (2002) 311–318.
[15] C. Cullis, B. Willatt, The inhibition of hydrocarbon oxidation over supported precious metal catalysts, J. Catal. 86 (1984) 187–200.
[16] S. Rasi, J. Läntelä, J. Rintala, Trace compounds affecting biogas energy utilisation—a review, Energy Convers. Manage. 52 (2011) 3369–3375.
[17] L.J. Hoyos, H. Praliaud, M. Primet, Catalytic combustion of methane over palladium supported on alumina and silica in presence of hydrogen sulfide, Appl. Catal. A 98 (1993) 125–138.
[18] T.-C. Yu, H. Shaw, The effect of sulfur poisoning on methane oxidation over palladium supported on γ-alumina catalysts, Appl. Catal. B 18 (1998) 105–114.
[19] D.L. Mowery, R.L. McCormick, Deactivation of alumina supported and unsupported PdO methane oxidation catalyst: the effect of water on sulfate poisoning, Appl. Catal. B 34 (2001) 287–297.
[20] P. Hurtado, Salvador Ordez, Herminio Sastre, V. Fernando, Combustion of methane over palladium catalyst in the presence of inorganic compounds: inhibition and deactivation phenomena, Appl. Catal. B 47 (2004) 85–93.
[21] Gélin Patrick, Michel Primet, Complete oxidation of methane at low temperature over noble metal based catalysts: a review, Appl. Catal. B 39 (1) (2002) 1–37.
[22] I. Rosso, Edoardo Garrone, Francesco Geobaldo, Barbara Onida, Guido Saracco, Vito Specchia, Sulphur poisoning of $LaMn_{1-x}Mg_xO_3$ catalysts for natural gas combustion, Appl. Catal. B 30 (2001) 61–73.
[23] J.J. Spivey, Complete catalytic oxidation of volatile organics, Ind. Eng. Chem. Res. 26 (1987) 2165–2180.
[24] CRC Handbook of Chemistry and Physics, in: W.M. Haynes, D.R. Lide, T.J. Bruno (Eds.), 94th ed., CRC Press, Boca Raton, Fla. [u.a.], 2013.
[25] J. Lampert, M. Shahjahan Kazi, Robert J. Farrauto, Palladium catalyst performance for methane emissions abatement from lean burn natural gas vehicles, Appl. Catal. B 14 (1997) 211–223.
[26] S. Ordóñez, Paloma Hurtado, Herminio Sastre, Fernando V. Díez, Methane catalytic combustion over Pd/Al_2O_3 in presence of sulphur dioxide: development of a deactivation model, Appl. Catal. A 259 (2004) 41–48.
[27] L.S. Escandón, S. Ordóñez, A. Vega, F.V. Díez, Sulphur poisoning of palladium catalysts used for methane combustion: effect of the support, J. Hazard. Mater. 153 (2008) 742–750.
[28] S. Ordóñez, P. Hurtado, F. Díez, Methane catalytic combustion over Pd/Al_2O_3 in presence of sulphur dioxide: development of a regeneration procedure, Catal. Lett. 100 (2005) 27–34.
[29] G.R. Lachance, F. Claisse, Quantitative X-ray Fluorescence Analysis: Theory and Application, New York, Wiley, Chichester, 1995.
[30] J.C. Lindon, G.E. Tranter, J.L. Holmes, Encyclopedia of Spectroscopy and Spectrometry, 3, Academic Press, San Diego, 2000.
[31] M. Torres Deluigi, J.A. Riveros, Chemical effects on the satellite lines of sulfur Kβ X-ray emission spectra, Chem. Phys. 325 (2006) 472–476.
[32] M. Kavčič, J.-C. Dousse, J. Szlachetko, W. Cao, Chemical effects in the Kβ X-ray emission spectra of sulfur, Nucl. Instrum. Methods Phys. Res. Sect. B 260 (2007) 642–646.
[33] R.A. Mori, E. Paris, G. Giuli, S.G. Eeckhout, M. Kavcic, M. Zitnik, K. Bucar, L.G.M. Pettersson, P. Glatzel, Sulfur-metal orbital hybridization in sulfur-bearing compounds studied by X-ray emission spectroscopy, Inorg. Chem. 49 (2010) 6468–6473.
[34] M. Mogi, A. Ota, S. Ebihara, M. Tachibana, M. Uda, Intensity analysis of S Kß emission spectra of Na2SO3 by the use of DV-Xα MO method, Nucl. Instrum. Methods Phys.Res. Sec. B 75 (1993) 20–23.
[35] M. Kavčič, A.G. Karydas, C. Zarkadas, Chemical state analysis employing sub-natural linewidth resolution PIXE measurements of Kα diagram lines, X-Ray Spectrom. 34 (2005) 310–314.
[36] A. Savitzky, M.J.E. Golay, Smoothing and differentiation of data by simplified least squares procedures, Anal. Chem. 36 (1964) 1627–1639.
[37] F.W. Knebel, Erdgasvorwärmung durch direkte katalytische Oxidation: Inline-Gasvorwärmung, in: Dissertation, Karlsruhe, 2000.
[38] U. Feuerriegel, Zur Desaktivierung eines Palladium-Trägerkatalysators durch Schwefelwasserstoff bei der katalytischen Methanoxidation, Dissertation, Kassel, 1993.
[39] O. Levenspiel, Experimental search for a simple rate equation to describe deactivating porous catalyst particles, J. Catal. 25 (1972) 265–272.
[40] G.F. Froment, Modeling of catalyst deactivation, Catal. Deactivation 212 (2001) 117–128.
[41] F. Ortloff, J. Bohnau, F. Graf, T. Kolb, Removal of oxygen from (bio-) methane via catalytic oxidation of CH4—reaction kinetics for very low O_2:CH_4 ratios, Appl. Catal. B: Environ. (2016), http://dx.doi.org/10.1016/j.apcatb.2015.09.026.